Received: 14 June 2021 | Revised: 31 August 2021 | Accepted: 15 September 2021

DOI: 10.1096/fj.202100936R

THE FASEB JOURNAL

RESEARCH ARTICLE

The pseudoprotease iRhom1 controls ectodomain shedding of membrane proteins in the nervous system

Johanna Tüshaus[1,2] | Stephan A. Müller[1,2] | Joshua Shrouder[3] | Martina Arends[1,4] | Mikael Simons[1,4,5] | Nikolaus Plesnila[3,5] | Carl P. Blobel[6,7,8] | Stefan F. Lichtenthaler[1,2,5]

[1]German Center for Neurodegenerative Diseases (DZNE), Munich, Germany

[2]Neuroproteomics, School of Medicine, Klinikum rechts der Isar, Technical University of Munich, Munich, Germany

[3]Institute for Stroke and Dementia Research (ISD), Klinikum der Universität München, Ludwig-Maximilians-University Munich, Munich, Germany

[4]Institute of Neuronal Cell Biology, Technical University Munich, Munich, Germany

[5]Munich Cluster for Systems Neurology (SyNergy), Munich, Germany

[6]Department of Physiology, Biophysics and Systems Biology, Weill Cornell Medicine, New York, New York, USA

[7]Department of Medicine, Weill Cornell Medicine, New York, New York, USA

[8]Arthritis and Tissue Degeneration Program, Hospital for Special Surgery, New York, New York, USA

Correspondence
Stefan F. Lichtenthaler, German Center for Neurodegenerative Diseases (DZNE), Feodor-Lynen-Str. 17, Munich 81377, Germany.
Email: stefan.lichtenthaler@dzne.de

Funding information
Deutsche Forschungsgemeinschaft (DFG), Grant/Award Number: EXC 2145 SyNergy,ID390857198 and FOR2290,263531414; Bundesministerium für Bildung und Forschung (BMBF), Grant/Award Number: CLINSPECT-M; HHS | National Institutes of Health (NIH), Grant/Award Number: R35 GM134907; Boehringer Ingelheim Fonds (BIF)

Abstract

Proteolytic ectodomain shedding of membrane proteins is a fundamental mechanism to control the communication between cells and their environment. A key protease for membrane protein shedding is ADAM17, which requires a non-proteolytic subunit, either inactive Rhomboid 1 (iRhom1) or iRhom2 for its activity. While iRhom1 and iRhom2 are co-expressed in most tissues and appear to have largely redundant functions, the brain is an organ with predominant expression of iRhom1. Yet, little is known about the spatio-temporal expression of iRhom1 in mammalian brain and about its function in controlling membrane protein shedding in the nervous system. Here, we demonstrate that iRhom1 is expressed in mouse brain from the prenatal stage to adulthood with a peak in early postnatal development. In the adult mouse brain iRhom1 was widely expressed, including in cortex, hippocampus, olfactory bulb, and cerebellum. Proteomic analysis of the secretome of primary neurons using the hiSPECS method and of cerebrospinal fluid, obtained from iRhom1-deficient and control mice, identified several membrane proteins that require iRhom1 for their shedding in vitro or in vivo. One of these proteins was 'multiple-EGF-like-domains protein 10'

Abbreviations: ADAMs, A disintegrin and metalloproteases; BACE1, β-site APP-cleaving enzymes 1; BTC, betacellulin; CNS, central nervous system; CSF, cerebrospinal fluid; DBCO, dibenzocyclooctyne; hiSPECS, high-performance secretome protein enrichment with click sugars; iRhom, inactive Rhomboid; MBP, myelin basic protein; MEFs, Mouse embryonic fibroblasts; MEGF10, multiple-EGF-like-domains protein 10; NFL, neurofilament light chain; PLP, myelin proteolipid protein; TGF, transforming growth factor.

(MEGF10), a phagocytic receptor in the brain that is linked to the removal of amyloid β and apoptotic neurons. MEGF10 was further validated as an ADAM17 substrate using ADAM17-deficient mouse embryonic fibroblasts. Taken together, this study discovers a role for iRhom1 in controlling membrane protein shedding in the mouse brain, establishes MEGF10 as an iRhom1-dependent ADAM17 substrate and demonstrates that iRhom1 is widely expressed in murine brain.

KEYWORDS

ADAM17, CSF, hiSPECS, iRhom1, myelination, secretome

1 | INTRODUCTION

Proteolytic ectodomain shedding of membrane proteins is essential for tissue homeostasis and cellular communication of multicellular organisms. During ectodomain shedding, the extracellular domain (ectodomain) of a membrane protein is proteolytically cleaved and secreted into the extracellular space and may be detected in body fluids. Shedding is mediated by various, mostly membrane-bound proteases, including a disintegrin and metalloproteases (ADAMs), β-site APP-cleaving enzymes (BACEs), meprin β, signal-peptide peptidase-like 3 and rhomboids.[1] Shedding acts as a molecular switch controlling abundance and function of hundreds of membrane proteins, including cell surface receptors, cell adhesion proteins, cytokines, and growth factors. When dysregulated, ectodomain shedding may lead to diseases, such as Alzheimer's disease, inflammation and cancer.[2–5] However, the molecular mechanisms controlling ectodomain shedding are only partly understood.

One major sheddase is ADAM17. This ubiquitously expressed metalloprotease has numerous membrane protein substrates and key functions in tissue homeostasis and epidermal growth factor receptor (EGFR) signaling.[6,7] Therefore, ADAM17-deficient mice resemble mice lacking the EGFR or selected EGFR ligands, such as transforming growth factor α (TGFα), and die shortly after birth.[6,8–11] Additionally, ADAM17 is a major therapeutic target for inflammatory diseases, because it also cleaves and controls the activity of the pro-inflammatory cytokine tumor necrosis factor (TNF)[9,12,13] and of the interleukin-6 receptor in immune cells.[7]

ADAM17 is regulated by non-proteolytic subunits, either inactive rhomboid 1 (iRhom1) or iRhom2 (also known as RHBDF1 and 2),[14–17] which may recruit a third binding partner, FRMD8/iTAP, to the iRhom/ADAM17 complex.[18,19] Both iRhoms belong to the larger family of intramembrane rhomboid proteins. While other rhomboids are active as serine proteases,[1,20] iRhom1 and iRhom2 lack the amino acids required for proteolytic activity and are referred to as pseudoproteases. iRhoms control multiple steps of the function and life-cycle of ADAM17, including the transport of ADAM17 from the endoplasmic reticulum to the plasma membrane and removal of its inhibitory propeptide,[14–17] its rapid activation by signaling pathways,[18,19,21,22] its substrate selectivity[23] and its stability and degradation.[24] The essential function of iRhoms for ADAM17 activity was revealed by iRhom1/2 double-deficient cells and mice which lack ADAM17 activity.[16,17] While iRhom1 and 2 are co-expressed in most cells and tissues and may have largely redundant functions during mouse development, there are two tissues in mice with predominant expression of only one iRhom.[25,26] Myeloid cells appear to express only iRhom2,[14,15,26] while the brain expresses predominantly iRhom1. The little iRhom2 detected in brain by qPCR derives from microglia, which are of myeloid origin.[16] Thus, iRhom1-deficient mice largely lack mature ADAM17 in the brain.[16] Yet, in contrast with iRhom2 and its specific functions and substrates in the immune system, little is known about the functions of iRhom1 and iRhom1-dependent shedding substrates in the brain.

Here, we discover a role for iRhom1 in controlling membrane protein shedding in the mouse brain, establish the phagocytic receptor 'multiple epidermal growth factor-like domains protein 10' (MEGF10) as an iRhom1-dependent ADAM17 substrate and demonstrate that iRhom1 is widely expressed in murine brain.

2 | MATERIALS AND METHODS

2.1 | Mouse work

Mouse work was performed according to the European Communities Council Directive (86/609/EEC) and was approved by the committee responsible for animal ethics of the government of Upper Bavaria (02-19-067). Mice were housed in the pathogen-free animal facility of the Center

for Stroke and Dementia Research (CSD) in Munich, Germany. *iRhom1*$^{-/-}$ mice[16] and *iRhom2*$^{-/-}$ mice (C57BL/6N-Rhbdf2$^{tm1b(KOMP)Wtsi}$/MbpMmucd) were used in this study. Heterozygous *iRhom1*$^{+/-}$ mice were mated in order to compare *iRhom1*$^{-/-}$ with littermate controls expressing wild-type full-length iRhom1 *(iRhom1*$^{+/+}$*)*.

2.2 | X-Gal staining

Due to a lack of iRhom antibodies suitable for expression analysis by immunohistochemistry or immunofluorescence, staining for X-Gal was performed. Adult iRhom1 (Rhbdf1tm1b(EUCOMM)Wtsi) and iRhom2 (KO C57BL/6N-Rhbdf2$^{tm1b(KOMP)Wtsi}$/MbpMmucd) mice, which express the lacZ gene under the control of their endogenous iRhom promoter,[16] or *iRhom1*$^{+/+}$ & *iRhom2*$^{+/+}$ control mice were sacrificed in a CO_2 chamber and perfused with PBS. Brains were isolated, fixed for 15 min on ice with 2% PFA and chopped into 2 mm thick sagittal brain sections or into hemispheres using a mouse brain slicer (Zivic instruments, BSMAS005-2). Sections were permeabilized for 1 h in permeabilization buffer (2 mM $MgCl_2$, 0.02% NP-40, in 1× PBS pH 7.4), before adding 1 mg/ml X-Gal, 2.12 mg/ml potassium ferrocyanide, and 1.64 mg/ml potassium ferricyanide together with fresh permeabilization buffer to perform the X-Gal staining overnight at 37°C.

2.3 | Western blotting

Brains were homogenized using a Precellys tissue homogenizer in combination with Hard Tissue homogenizing CK28 tubes as previously described.[27] Brain homogenates were lysed in 1 ml and neurons of a 6-well were lysed in 200 µl 1%-Triton lysis buffer (50 mM Tris-HCl pH 7.5 with 150 mM NaCl, 1 mM EDTA, 1% Triton X-100, 10 mM 1–10 phenanthroline, 1:500 protease inhibitors cocktail).[28] Membrane fractions of brain homogenates were enriched as previously described.[29] Total protein concentration was measured using Pierce BCA Protein Assay Kit. The samples were typically boiled for 10 min at 95°C in 1× reducing Laemmli buffer containing β-mercaptoethanol before loading onto self-made 8%–12% Tris-glycine gels. However, samples for iRhom1 blots were not boiled to prevent aggregation of this multi-pass transmembrane protein. Samples for ADAM17 blots were enriched using Concanavalin A agarose beads (Sigma, C7555) before boiling the beads in Laemmli buffer[14] to reduce background bands which can interfere with the detection of ADAM17 by Western blot analysis. SDS-PAGE was performed, proteins were transferred onto nitrocellulose membranes, blocked for 30 min at room temperature with 5% milk powder in 1× PBS with 0.5% Tween. Primary antibodies were incubated overnight at 4°C while the secondary antibodies were added for 1 h at room temperature. The following primary antibodies were used: anti-iRhom1 (20A8, rat, N-term),[30] anti-ADAM10 (rabbit, C-term, Abcam, EPR5622), anti-ADAM17 (rabbit, C-term),[31] anti-BACE1 (3D5, mouse, kindly provided by Robert Vassar), anti-β-actin (mouse, Sigma, AC-74), anti-Calnexin (rabbit, Enzo Life Sciences, ADI-SPA-860).

2.4 | Myelination analysis

Six-weeks-old *iRhom1*$^{-/-}$ mice and littermate *iRhom1*$^{+/+}$ controls were anesthetized with isoflurane and perfused with 4% PFA in PBS. The vertebral columns were removed, immersion fixed in 4% PFA overnight and soaked in 30% Sucrose for 2 days for cryoprotection. After the spinal cords were carefully removed from the vertebral columns, they were embedded in OCT (Tissue-Tek), frozen on dry-ice and stored at −80°C. Cervical spinal cord sections (14 µm) were cut transversely by cryostat (Leica) and mounted directly on Superfrost Plus slides (ThermoFisher Scientific). All sections were stored at −20°C until further processing. For immunohistochemistry, the sections were washed with 1× PBS and permeabilized with 0.3% Triton X-100 in PBS for 10 min. To prevent unspecific binding, tissue sections were first blocked with donkey anti-mouse Fab fragments (Jackson ImmunoResearch) and then with blocking solution containing 2.5% Fetal Bovine Serum, 2.5% Bovine Serum Albumin, and 2.5% fish gelatin in PBS for 1 h. Sections were stained for chicken anti-MBP (1:1000, ThermoFisher Scientific, PA1-10008), mouse anti-PLP (1:500, Bio-Rad, MCA839G) and rabbit anti-neurofilament 200 (1:500, Sigma-Aldrich, N4142). Primary antibodies were diluted in blocking solution and incubated overnight at 4°C. After washing the sections with 1× PBS, secondary antibodies were applied for 2 h. We used Alexa Fluor 488-, 555-, and 647-conjugated secondary antibodies (ThermoFisher Scientific). The sections were washed with 1× PBS. DAPI was applied for 15 min. After final washing with 1× PBS and distilled water, the sections were mounted with ProLong Diamond Antifade (ThermoFisher Scientific). Unless stated otherwise, all steps were performed at room temperature. A confocal laser-scanning microscope (Leica TCS SP5) was used for image acquisition. We analyzed the integrated density per mm^2 in the white and grey matter of three animals with 4–5 spinal cord sections per animal by using ImageJ/Fiji and Graphpad Prism 8. Differences were tested with multiple *t*-tests assuming Gaussian distribution.

2.5 | Vessel density in adult mice

iRhom1$^{-/-}$ mice and littermate *iRhom1*$^{+/+}$ control mice aged between 6 and 13 weeks were injected with triple combination [medetomidine, midazolam, and fentanyl (0.05/5/0.5 mg/kg i.p.)] as a terminal anesthetic before transcardial perfusion with 200 μl of lectin [20 mg/ml, Lycopersicon Esculentum (Tomato) Lectin, L32470, ThermoFischer] into the left ventricle. The needle tip was held inside the heart for 3 min to allow the lectin to circulate and stain the vasculature before 5 min of perfusion with saline to remove the blood and 5 min of 4% PFA perfusion fixation. Brains were then removed and stored in 4% PFA overnight before being transferred to PBS. Serial coronal sections 50 μm thick were cut at the vibratome and stained for Goat anti-albumin in primary antibody buffer (1% BSA, 0.1% Fish-skin gelatin, 0.1% Triton X-100, 0.05% Tween 20 in 1× PBS) at a concentration of 1:500 on a rotary shaker O/N at 4°C. The next day, sections were washed thoroughly in 1× PBS and stained with Donkey anti-goat 594 at a concentration of 1:300 in secondary antibody buffer (2% BSA, 2% FCS, 0.2% Fish-skin gelatin diluted down in 1× PBS). Slices were then stained 1:1000 with DAPI for 30 min washed 3× in PBS and mounted onto a glass slide and coverslip with Everbrite™ mounting medium and sealed with nail varnish before imaging at the Zeiss Axio imager M2 microscope. After imaging four brain slices per animal, four regions of interest (ROIs) were randomly selected in the striatum and cortex in each slice respectively. From these ROIs, the lectin channel was recorded and analyzed in FIJI. To calculate vessel density, the lectin channel was thresholded to match the existing vessel signal and create a black vessel mask from which the number of black pixels corresponded to vessel density/image.

2.6 | Pericyte coverage analysis in *iRhom1*$^{-/-}$ mice

iRhom1$^{-/-}$ mice and littermate *iRhom1*$^{+/+}$ controls were terminally anesthetized with medetomidine, fentanyl and midazolam, and transcardially perfused with lectin followed by ice cold saline for 5 min and 4% PFA for another 5 min. Brains were removed and sectioned serially using a vibratome into 50 μm thick brain sections. Sections were stained for anti-goat PDGFRβ (AF1042, R&D systems) in primary antibody buffer (1% BSA, 0.1% Fish-skin gelatin, 0.1% Triton X-100, 0.05% Tween 20 in 1× PBS) overnight at 4°C on a rotary shaker. Slices were then washed 3× in PBS for 30 min to remove unbound primary antibodies and stained with Donkey anti-goat Alexa fluor 594 (1:300) antibodies in secondary antibody buffer (2% BSA, 2% FCS, 0.2% Fish-skin gelatin diluted down in 1× PBS) overnight at 4°C on a rotary shaker. Slices were then washed twice for 30 min in 1× PBS before adding DAPI at 1:1000 for 30 min and the washing steps were repeated. Slices were mounted on glass slides with Everbrite™ mounting medium and sealed with a glass coverslip and nail varnish before imaging by confocal fluorescence microscopy. Five ROIs were randomly selected in two brain slices in both the striatum and cortex and *z* stacks were collected and the maximum intensity was projected to display pericyte coverage on lectin covered vessels. Vessel density was analyzed as previously described. Using PDGFRβ+ pixels as a guide, pericytes and their processes were thresholded and the resultant signal area was divided over vessel density/ROI to generate pericyte coverage per striatal and cortical region respectively.

2.7 | ELISA

Soluble APPβ levels were determined in the secretome of primary cultured neurons using the sAPPβ-wild-type (mouse) ELISA (TECAN, #JP27416) according to manufacturer's instructions. Cultivation media of 1.5 Million neurons was collected for 48 h from DIV 5 to 7. Each sample was analyzed as technical duplicates using 100 μl cultivation media each ($N = 6$).

2.8 | Cell culture

Cell lines as well as primary cells were cultured under standard conditions at 37°C and 5% CO_2. *Adam17*$^{-/-}$ and *Adam17*$^{+/+}$ mouse embryonic fibroblasts (MEFs)[32] were maintained with culture medium (DMEM medium supplemented with 1% Penicillin-Streptomycin and 10% FBS) on Poly-D-Lysine coated dishes. Primary cortical/hippocampal neurons were isolated from single embryos at embryonic day 16 if derived from a heterozygous mating as described previously.[33,34] In brief, both cortex and hippocampus of each hemisphere were collected in a 1.5 ml tube after complete removal of the meninges. The tissue was incubated for 15 min in the cell culture incubator at 37°C in pre-activated digestions medium (200 U papain in DMEM with 1 μg/μl L-cysteine; Papain activation took place at 37°C for 30 min). Next, the tissue was mechanically dissociated in culture medium, live cell counting was performed on an automated cell counter (BioRad) with trypan blue staining and 1.5 × 10^6 living cells were seeded into Poly-D-Lysine coated wells of a 6-well plate. Three hours post seeding, cultivation media was exchanged to neuronal growth medium (Neurobasal Medium supplemented with 1% Penicillin-Streptomycin,

5 mM GlutaMAX and 2% B27). Medium and supplements were purchased from Gibco ThermoFisher.

2.9 | hiSPECS analysis

Secretome analysis of primary neuronal cultures was performed using the 'high-performance secretome protein enrichment with click sugars' (hiSPECS) method, described in detail previously.[35] In brief, neurons were cultured for 48 h (DIV 5–7) in the presence of 50 μM ManNAz (#88904, ThermoFisher), cultivation media was filtered through 0.45 μm spin columns (Sigma-Aldrich, CLS8163). Glycoproteins were enriched using ConA agarose beads (Sigma, C7555) and clicked to magnetic dibenzocyclooctyne (DBCO) beads (Jena Bioscience, CLK-1037). Peptides were released from the beads by on-bead tryptic digest and were desalted using the stage tip protocol.[36] Finally, peptides were dissolved in a total volume of 20 μl (18 μl 0.1% FA with 2 μl iRT peptides (1:10, Ki-3002-1, Biognosys)) of which 8 μl were injected per LC-MS/MS run.

2.10 | CSF isolation

The CSF was isolated from *iRhom1*$^{-/-}$ mice and *iRhom1*$^{+/+}$ control littermates at the age of 3 months ($N = 4$) following a previously described procedure.[37,38] Mice were anesthetized with a cocktail of medetomidine, midazolam, and fentanyl (0.05/5/0.5 mg/kg i.p.). Next, the mice were positioned into a stereotaxic frame, the cisterna magna was exposed and a glass capillary was used to puncture the dura and to harvest the CSF by applying slight negative pressure. The blood-free CSF samples were cleared by centrifugation at 3000 *g* for 20 min and snap-frozen in liquid nitrogen. 5 μl CSF was used for in-solution digestion including sodium deoxycholate as described by Ref. [29]

2.11 | Mass spectrometry

All mass spectrometry measurements were conducted on an EASY-nLC 1200 UHPLC system (Thermo Fisher Scientific) connected to a Q-Exactive™ HF Hybrid Quadrupole-Orbitrap™ mass spectrometer (Thermo Fisher Scientific) as described.[39] Peptides were separated on self-packed 30 cm long C18 columns (ReproSil-Pur 120 C18-AQ resin Dr Maisch GmbH) with a diameter of 75 μm. CSF samples were analyzed using data-dependent acquisition (DDA) using the MaxQuant software[40] (1% FDR on protein and peptide level). Whereas hiSPECS secretome samples were analyzed using data-independent acquisition (DIA) in combination with self-generated hiSPECS neuronal secretome library[35] using Spectronaut Pulsar.[41] Details of the chromatography (120-min gradient) and mass spectrometry parameters were set as described.[35] Proteomic data are accessible via PRIDE with the following project accession: PXD028096.

2.12 | Shedding assay

Alkaline phosphatase (AP)-shedding assays were performed in *ADAM17*$^{+/+}$ and *ADAM17*$^{-/-}$ MEFs as described.[22] In brief, cells were seeded onto Poly-D-Lysine coated 12-well plates at a density of 2×10^5 cells per well. 16 h post seeding, cells were transfected with AP-tagged ADAM17 substrate candidates (AP5 plasmid) using Lipofectamine-2000 (ThermoFisher, 11668027; 1 μg Plasmid, 2 μl Lipofectamine-2000, 2 × 100 μl Opti-MEM). On the next day, a PMA stimulation step was conducted with two of the four technical replicates. Cells were cultured for 1 h in Opti-MEM, stimulated for 45 min with/without 25 ng/ml PMA in Opti-MEM and finally cells were lysed in 2.5% Triton-Lysis buffer (1 mM EDTA, 2.5% Triton-X100 in ddH_2O). Both, cultivation medium and lysate, were cleared by centrifugation at maximum speed for 10 min prior to adding the AP substrate 4-nitrophenyl phosphate. AP activity was determined in triplicates by measuring the absorbance at 405 nm. The ratio of AP activity in the cultivation medium relative to the overall AP activity in lysate and cultivation medium was assessed and each experiment was repeated at least three times. TGF-α served as positive, BTC as negative control for ADAM17 shedding activity and the following primers were used for cloning the substrate candidates (EphB6, Mrc2, Megf10, Sema5b) into the AP5 backbone:

Gene name	Direction	Sequence 5′-3′
EphB6	F	TAAGCA GTCGACACCATGACCAGTGAGACC
	R	TGCTTAGCTAGCGACACTTCCACTGAGCCTGG
Megf10	F	TAAGCA CTCGAGTGCCCTGCGGGAACATAC
	R	TGCTTAGCTAGCGA TTCACTGCTGCTGCTGCT

Gene name	Direction	Sequence 5′-3′
Mrc2	F	TAAGCACTCGAGGTCTGGCAAGACAACACA
	R	TGCTTATCTAGAGATTCTTGCTGT TCGTTCAT
Sema5b	F	TAAGCAGTCGACTCTGAGTGGGGTGTCTGC
	R	TGCTTATCTAGAGAGCTGTTGGGGAAACAGCG

3 | RESULTS

3.1 | Analysis of iRhom1 expression in mouse brain

We analyzed iRhom1 expression in the mouse brain in a spatially resolved manner. Because there are no antibodies available against iRhom1 that are suitable for immunohistochemistry, we used one of the four previously generated iRhom1-deficient mouse lines, in which the endogenous promoter of iRhom1 drives the expression of the β-galactosidase gene lacZ.[16] Additionally, we used a similar iRhom2 reporter mouse line expressing lacZ under the endogenous promoter of iRhom2 (C57BL/6N-Rhbdf2$^{tm1b(KOMP)Wtsi}$/MbpMmucd). The enzyme β-galactosidase is able to convert the dye X-gal to a blue indigo-based dye, allowing to visualize the localization of β-galactosidase activity. Addition of X-gal to brains and brain slices from *iRhom1*-deficient mice revealed that *iRhom1* is widely expressed in the murine brain with highest expression in the olfactory bulb, cerebral cortex, cerebellum, and the dentate gyrus of the hippocampus (Figure 1A). Interestingly, limited expression of iRhom2 was observed in the adult mouse brains (Figure 1A) which is in agreement with previous RNA expression studies of iRhom2.[16,17] As control, wild-type (*iRhom1*$^{+/+}$ & *iRhom2*$^{+/+}$) mice, which did not express lacZ, did not show any blue staining (Figure 1A).

To analyze iRhom1 expression in the mouse brain in a time-resolved manner, we used immunoblots and first verified the specificity of the iRhom1 antibody by demonstrating that the iRhom1 protein band at around 100 kDa was not detected in brain homogenates from *iRhom1*$^{-/-}$ mice compared to *iRhom1*$^{+/+}$ littermate controls (Figure 1B). iRhom1 expression was detected from embryonic stage (E16.5) to adulthood with a peak of expression in the first two weeks after birth (Figure 1C). To determine the expression of iRhom1 in different brain cell types, we could not use immunohistochemistry, because our antibody is not suitable for this application. Instead, we extracted expression information from a protein resource[42] and from the Brain RNA-Seq database.[43] Both datasets revealed iRhom1 expression in the major brain cell types, with strong expression of iRhom1 in astrocytes and lower expression in oligodendrocytes and neurons (Supporting Information Figure S1). iRhom1 protein was not detected in microglia from newborn, but from adult mice (Supporting Information Figure S1A) and iRhom1 RNA was also seen in microglia from very young mice (Supporting Information Figure S1B).

The absence of iRhom1 protein in the brain of *iRhom1*$^{-/-}$ mice was accompanied by a strong reduction of the mature, proteolytically active form of ADAM17 (Figure 1B), in agreement with a previous report.[16] Because ADAM17 has been functionally linked to myelination in the nervous system (CNS)[44–46] and because iRhom1 expression is high in the postnatal period when myelination occurs, we tested the possibility that *iRhom1*$^{-/-}$ mice have changes in the extent of myelination. However, in cervical spinal cord sections of six weeks old *iRhom1*$^{-/-}$ mice compared to littermate control mice we did not observe obvious changes (Supporting Information Figure S2). ADAM17 also has a function in blood vessel formation,[47,48] but the *iRhom1*$^{-/-}$ mice revealed no major changes in vessel density and pericyte coverage in the brain (Supporting Information Figure S3).

We conclude that iRhom1 is widely expressed in the murine brain with higher levels in astrocytes and lower levels in other brain cell types, has an expression peak in the postnatal period and is essential for ADAM17 maturation in the brain. However, despite a link of ADAM17 to myelination and blood vessel formation, the iRhom1$^{-/-}$ mouse line analyzed in our study did not show obvious changes in myelination or cerebral blood vessel density.

3.2 | iRhom1-deficiency reduces shedding of membrane proteins in primary neurons

When ADAM17 cleaves membrane protein substrates, their ectodomains are secreted from cells into the extracellular space, where they are found together with soluble, secreted proteins. Together, the shed ectodomains and the soluble, secreted proteins constitute the cellular secretome. To test for a role of iRhom1 in membrane protein shedding in the brain, we used mass spectrometry-based proteomics and quantitatively determined how

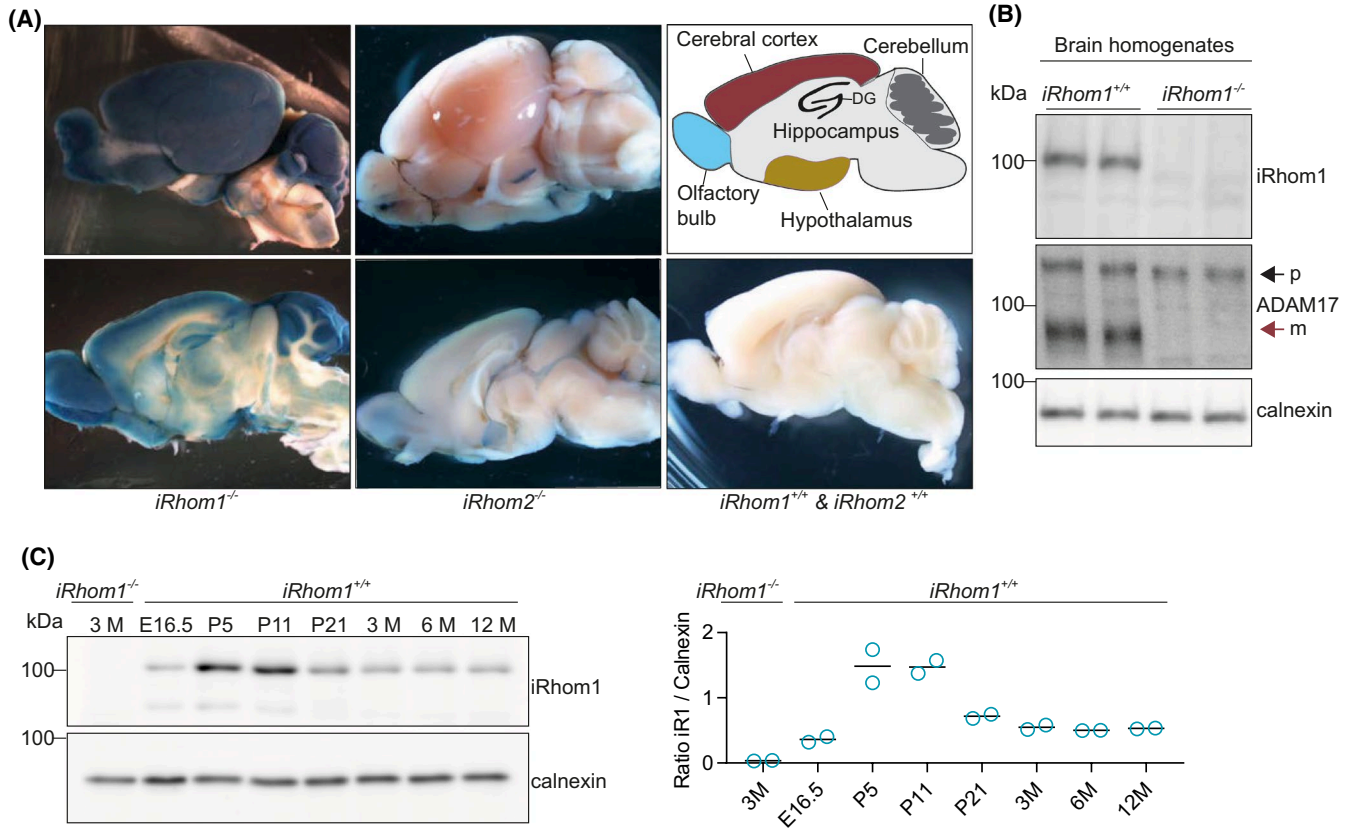

FIGURE 1 iRhom1 expression in the murine brain. (A) X-Gal staining of brain slices of adult *iRhom1*$^{-/-}$, *iRhom2*$^{-/-}$, and control (*iRhom1*$^{+/+}$, *iRhom2*$^{+/+}$) mice ($N = 3$). (B) Comparison of ADAM17 maturation by Western blot analysis of brain homogenates of *iRhom1*$^{-/-}$ mice and *iRhom1*$^{+/+}$ littermate controls at the age of 3 months ($N = 4$). The black arrow indicates the immature (p, proform/inactive) and the red arrow the mature (m, active) form of ADAM17. (C) Western blot analysis of brain homogenates of mice of different ages revealing iRhom1 protein abundance during development ($N = 2$). The quantification of the iRhom1 (iR1) signal relative to calnexin is shown

the lack of iRhom1 affects protein abundance in the secretome of primary neurons, which is the brain cell type with the largest number of shed membrane proteins.[35] We used 1.5 million primary murine neurons isolated from single embryos (E16.5) of *iRhom1*$^{-/-}$ or *iRhom1*$^{+/+}$ littermate control mice and determined the secretome with the proteomic hiSPECS (high-performance secretome protein enrichment with click sugars) method[33,35] (Figure 2A), which was successfully used for substrate identification of several shedding proteases.[33,35,49,50] For hiSPECS analysis, neurons were metabolically labeled with a chemically modified azide-sugar that is integrated into newly synthesized *N*-glycosylated secreted soluble and membrane proteins. This modification allows to culture the primary neurons in the presence of abundant serum proteins, such as albumin, required for their survival, but enables a specific purification of the lower-abundant cell-derived secretome proteins from the conditioned medium for subsequent mass spectrometric analysis (Figure 2A).

Similar to whole brain (Figure 1B), *iRhom1*$^{-/-}$ neurons lacked the mature form of ADAM17 (Figure 2B). The Pearson correlation coefficient of the log2 LFQ values of all proteins detected in the neuronal secretomes revealed high reproducibility between the biological samples with an average value of 0.928 (Figure 2C for a representative graph; all graphs in Supporting Information Table S1). In total, 409 proteins were quantified in four of six biological replicates in at least one group, of which 77% were annotated as glycoproteins according to UniProt (Figure 2D). 196 proteins were annotated as single-pass transmembrane or GPI-anchored proteins (Supporting Information Table S1). We consider them as potentially shed proteins (Figure 2D), because the secretome of primary neurons mostly contains the ectodomain of such membrane proteins, but not their full-length forms.[35] To identify among them the potential iRhom1-dependent substrates we looked for transmembrane proteins having a significantly reduced ectodomain abundance in the neuronal *iRhom1*$^{-/-}$ secretome (Figure 2E). This yielded 14 proteins (ADAM9, BCAM, CADM4, CNTNAP5A, ENPP5, LRRC4, MEGF10, MEGF11, OMG, P10404/MLV-related proviral Env polyprotein, PLD3, PTPRM, PTPRU,

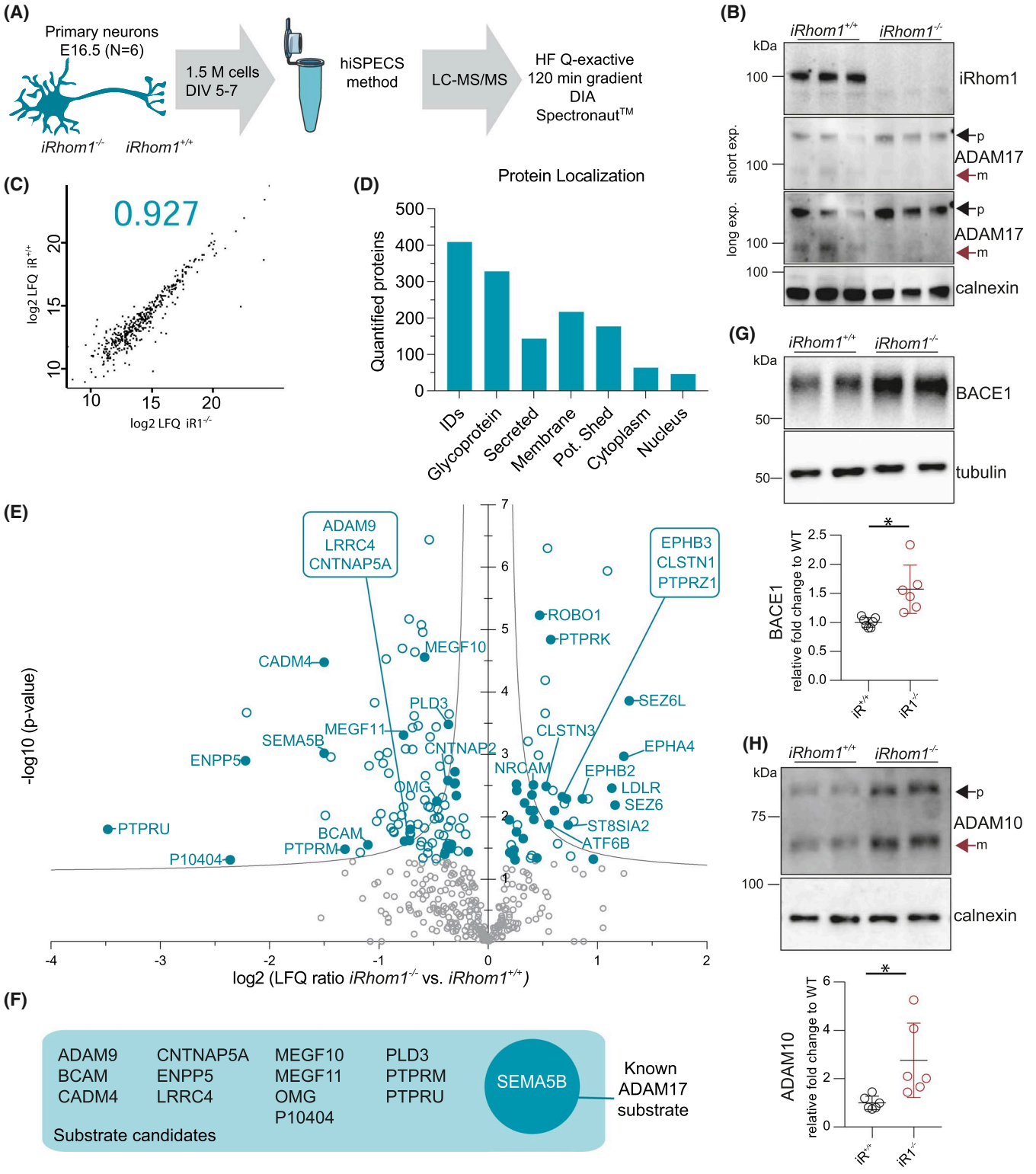

SEMA5B) annotated as single-pass or GPI-anchored membrane proteins (Figure 2F, Table 1, Supporting Information Table S1), indicating that their shedding requires iRhom1. One of them, SEMA5B is a known ADAM17 substrate,[51] suggesting that also the other iRhom1-dependent shed membrane proteins are likely to be ADAM17 substrates in primary neurons.

Surprisingly, an increased shedding was observed for 15 transmembrane proteins in the secretome of *iRhom1*$^{-/-}$ neurons (Figure 2E, Supporting Information Table S1), including established substrates of the Alzheimer's disease-linked protease BACE1 (also known as β-secretase) (SEZ6, SEZ6L)[29,52] and the ADAM17-related protease ADAM10 (NRCAM, LDL-R, PTPRK).[50,53] The Alzheimer's

FIGURE 2 Secretome analysis of *iRhom1*$^{-/-}$ neurons. (A) Workflow of the proteomic hiSPECS secretome analysis comparing *iRhom1*$^{-/-}$ neurons to *iRhom1*$^{+/+}$ neurons isolated from littermate control embryos at E16.5 ($N = 6$). (B) Western blot analysis of *iRhom1*$^{-/-}$ and *iRhom1*$^{+/+}$ neurons. The black arrow indicates the immature (p, proform/inactive) and the red arrow the mature (m, active) form of ADAM17. A short and a long exposure (exp.) time of the same blot is shown. (C) Representative Pearson correlation coefficient of log2 label-free quantification (LFQ) values of all quantified proteins in the neuronal secretome upon mass spectrometric analysis. Individual coefficients for all experiments are given in Supporting Information Table S1. (D) Number of proteins quantified in at least one group in four of six biological replicates and their distribution according to cellular localization on UniProt. Proteins with a single transmembrane domain or a GPI-anchor were grouped as potentially shed proteins. (E) Volcano plot depicting the log2 abundance change in the secretome of *iRhom1*$^{-/-}$ compared to littermate control *iRhom1*$^{+/+}$ neurons and the negative log10 *p*-value for each protein (two-sample *t*-test, $N = 6$). Permutation-based false discovery rate (FDR, $p = 0.05$, $s_0 = 0.1$) estimation is visualized with the grey hyperbolic curves. Proteins with a *p*-value below .05 are highlighted with a blue circle and potentially shed proteins with a filled circle (reduced blue, increased pink). (F) Potential ADAM17 substrate candidates which show a significant reduction (*p*-value < .05) in *iRhom1*$^{-/-}$ neuronal secretome (14 proteins). The substrate Sema5B is known to be cleaved by ADAM17 and is highlighted with white letters. (G, H) Western blot analysis of neuronal lysate for BACE1 and tubulin (G) or ADAM10 and calnexin (H). Signals were normalized to the loading control (calnexin, tubulin) and to the average of the *iRhom1*$^{+/+}$ control samples using a one sample *t*-test and applying the significance criterion *p*-value < .05 (BACE1 $p = .02$, ADAM10 $p = .038$). Both bands of ADAM10 were considered for the quantification

TABLE 1 List of the significantly (FDR curve: $p = .05$; s0 = 0.1) reduced potentially shed proteins detected in the secretome of *iRhom1*$^{-/-}$ versus *iRhom1*$^{+/+}$ neurons

ProteinAC	Gene name	*p*-value	Fold change KO versus WT	Topology	AD17 substrate	CSF analysis
B1AUH1	Ptpru	1.58E−02	0.09	TM1		n.d.
P10404	P10404	4.89E−02	0.20	TM1		n.d.
Q9EQG7	Enpp5	1.25E−03	0.21	TM1		n.d.
Q8R464	Cadm4	3.34E−05	0.35	TM1		d.
Q60519	Sema5b	9.55E−04	0.35	TM1	+	n.d.
P28828	Ptprm	3.30E−02	0.40	TM1		n.d.
Q9R069	Bcam	2.83E−02	0.47	TM1		d.
Q80T91	Megf11	4.91E−04	0.58	TM1		n.d.
Q99PH1	Lrrc4	2.45E−02	0.59	TM1		n.d.
Q61072	Adam9	2.38E−02	0.61	TM1		n.d.
Q0V8T9	Cntnap5a	1.59E−02	0.61	TM1		n.d.
Q6DIB5	Megf10	2.75E−05	0.67	TM1		sign. red.
Q63912	Omg	5.68E−03	0.72	GPI		d.
O35405	Pld3	3.29E−04	0.78	TM2		d.

Abbreviations: d., detected; FDR, false discovery rate; GPI, GPI-anchored protein; n.d., not detected; sign. red.: significantly reduced; TM1, transmembrane protein type 1; TM2, transmembrane protein type 2.

disease-linked protein APP is a substrate for both ADAM10 and BACE1, but did not show a significant change of its secreted ectodomain (sAPP) in the conditioned medium of the *iRhom1*$^{-/-}$ neurons, based on the hiSPECS analysis (Supporting Information Table S1). Because this mass spectrometric analysis is not able to distinguish between the ADAM10 and BACE1 cleavage products of APP (sAPPα and sAPPβ), we used an ELISA that specifically detects murine sAPPβ and observed that sAPPβ levels were not significantly changed in the secretome of *iRhom1*$^{-/-}$ and *iRhom1*$^{+/+}$ primary neurons (Supporting Information Figure S5). This indicates that not all BACE1 substrates show increased shedding in *iRhom1*$^{-/-}$ neurons.

While a molecular connection of iRhom1 to BACE1 or ADAM10 is not known, it is interesting to note that the lack of iRhom1 increased ADAM10 (2.76-fold) and BACE1 (1.57-fold) protein levels in the *iRhom1*$^{-/-}$ versus *iRhom1*$^{+/+}$ neurons (Figure 2G,H), indicating a potential compensatory upregulation of both proteases in the absence of neuronal iRhom1 or of mature, proteolytically active, neuronal ADAM17. However, a similar increase in ADAM10 and BACE1 levels was not seen in membrane fractions from whole brains of adult, 3 month-old mice (Supporting Information Figure S4), and may thus, only be relevant in neurons, but not in the other brain cell types, which outnumber neurons in adult mouse brain, or

may be an effect restricted to the culture of primary neurons and not be visible in vivo.

Besides the shed membrane proteins, 27 proteins annotated as soluble secreted proteins were found to be significantly down- or upregulated in the *iRhom1*$^{-/-}$ secretome (Figure 2E and Supporting Information Table S1). Because these proteins are not membrane proteins and, thus, do not require shedding, their changed abundance is likely an indirect consequence of iRhom1-deficiency in the neurons.

Thus, we conclude that loss of iRhom1 leads to a pronounced change in the neuronal secretome, demonstrating that iRhom1 has a function in neuronal ectodomain shedding, but also in the release of soluble, secreted proteins.

3.3 | ADAM17 substrates have reduced abundance in cerebrospinal fluid from *iRhom1*$^{-/-}$ mice

Next, we analyzed whether iRhom1-dependent membrane protein shedding can also be detected in vivo in the brain. To that aim, we used cerebrospinal fluid (CSF), which is the body fluid in direct contact with the brain and constitutes an in vivo brain secretome. CSF does not only contain proteins of neuronal origin, but also from other brain cell types.[35] CSF protein abundance was measured and quantified using mass spectrometry-based proteomics (Figure 3A). Because CSF can only be taken from adult mice, we took the iRhom1-deficient mouse line which was also used for the X-gal stainings (Figure 1A), because this model reveals no enhanced lethality compared to control mice.[16] The average Pearson correlation coefficient for the protein abundance quantification between all samples was 0.931 and indicates very good reproducibility (Figure 3B for representative graph, all graphs in Supporting Information Table S1). In total, we quantified 669 proteins in at least three of four biological replicates of either *iRhom1*$^{+/+}$ control or *iRhom1*$^{-/-}$ CSF. This number of quantified proteins is similar to other proteomic, murine CSF studies.[29,35] 201 of the 669 quantified proteins were annotated as single-pass transmembrane or GPI-anchored proteins according to UniProt (Supporting Information Table S1) and, thus, are potentially shed membrane proteins (Figure 3C).

33 proteins showed reduced or increased CSF abundance, when applying a *t* test *p*-value < .05 (Figure 3D). Yet, none of the proteins reached the more stringent significance criterion when using false-discovery rate (FDR) correction for multiple hypothesis testing (1%) (Figure 3D). Thus, we considered those proteins as potential hits which had a *t*-test-based *p*-value < .05 and a log2-fold-change >0.5 in *iRhom1*$^{-/-}$ CSF compared to *iRhom1*$^{+/+}$ CSF (vertical lines in Figure 3D). This yielded 20 proteins, with 14 having reduced CSF abundance and six proteins showing increased CSF abundance (Table 2). Among the proteins with reduced CSF abundance were six proteins annotated as transmembrane proteins (EphB6, LAG3, LDLR, MEGF10, Mrc2, NCAM2) and their detected, tryptic peptides mapped exclusively to their ectodomains (Figure 3F), as expected for a shed membrane protein. The six proteins included LAG3, a known ADAM17 substrate[54] and MEGF10 which also had reduced levels in the *iRhom1*$^{-/-}$ neuronal secretome (Figure 3E). Thus, we conclude that MEGF10 is an iRhom1-dependent shedding substrate both in vitro and in vivo (Figures 2E and 3D). Several membrane proteins identified in the primary neuron secretome (Table 1) as potential iRhom1-dependent shedding substrates were not detected in CSF (ADAM9, CNTNAP5A, ENPP5, LRRC4, MEGF11, P10404 (MLV-related proviral Env polyprotein), PTPRM, PTPRU, SEMA5B), probably because their abundance was below the detection limit in the CSF, so that they cannot be confirmed in vivo at this point. Other iRhom1-dependent shedding substrates from the primary neuron analysis, however, were detected but not changed (BCAM, CADM4, OMG, PLD3), potentially because in vivo they are not only shed from neurons but also from other brain cell types where they may be shed in an ADAM17/iRhom1-independent manner.

Six proteins with reduced CSF abundance (CHGA, DKK3, EFEMP1, GM1673, NCAN, SVEP1) as well as the five proteins with increased CSF abundance (CHI3L1, LBP, LGALS3BP, ORM1, RARRES2) are known soluble, secreted proteins (according to UniProt) with the exception of THMSB4X, which is annotated as a soluble cytoplasmic protein. Because of their lack of a transmembrane domain, these proteins do not require shedding and, thus, are likely to be reduced or increased as a secondary consequence of iRhom1-deficiency.

In conclusion, the CSF analysis demonstrates that iRhom1 controls CSF abundance of selected membrane and soluble proteins, including MEGF10, which was also identified as an iRhom1-dependent shedding substrate in primary neurons.

3.4 | Validation of novel iRhom1-dependent substrates as being cleaved by ADAM17

Next, we validated the proteomic results from the iRhom1-deficient CSF and neuronal secretome by an independent method using selected substrate candidates

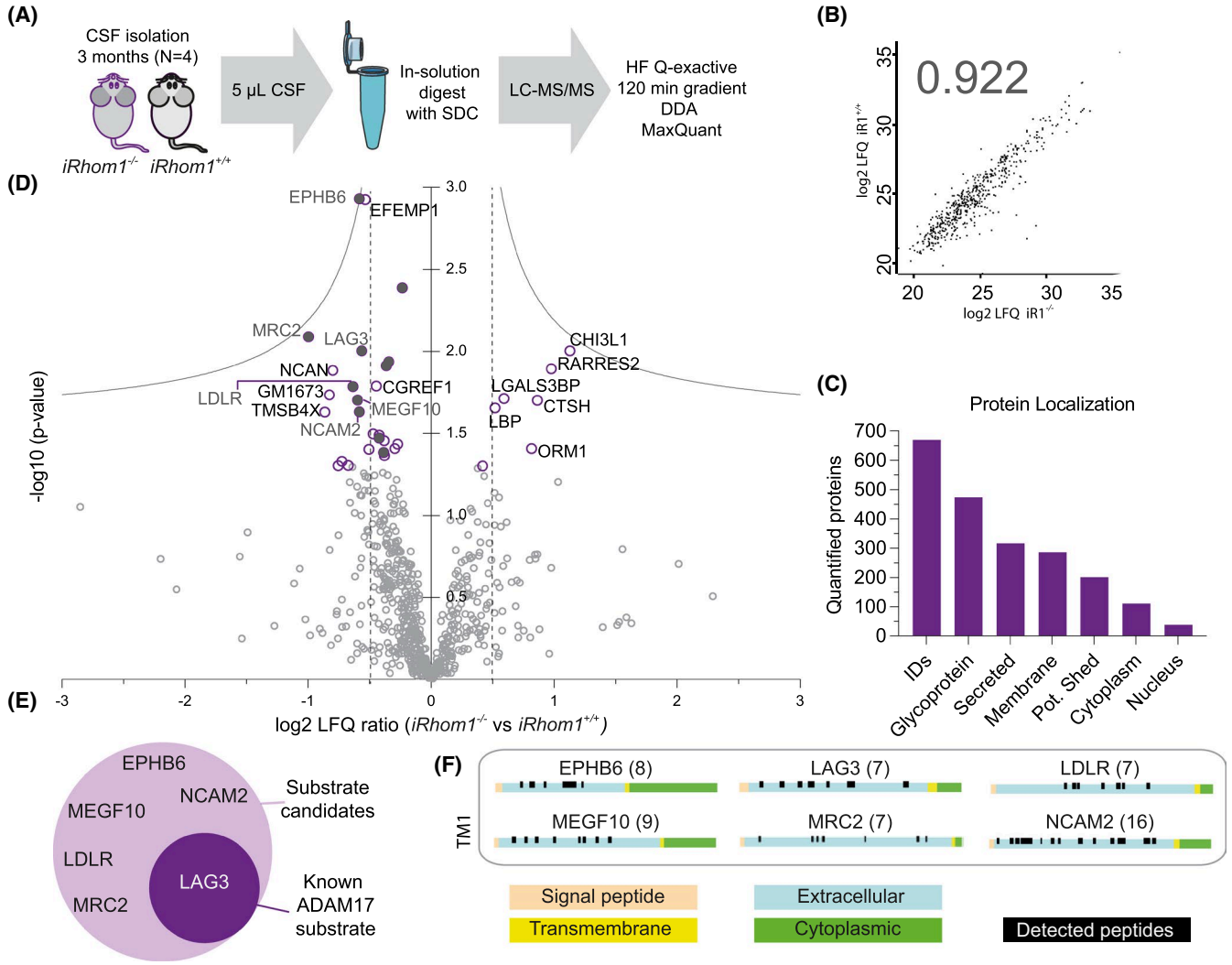

FIGURE 3 CSF analysis of *iRhom1*$^{-/-}$ mice. (A) Workflow of the proteomic CSF analysis comparing *iRhom1*$^{-/-}$ mice to littermate controls (*iRhom1*$^{+/+}$) at the age of 3 months ($N = 4$). (B) Representative Pearson correlation coefficient of log2 LFQ values of all quantified proteins. Individual coefficients for all experiments are given in Supporting Information Table S1. (C) Number of proteins quantified in at least one group in three of four biological replicates and their distribution according to cellular localization on UniProt. Proteins with a single transmembrane domain or a GPI-anchor were grouped as potentially shed proteins. (D) Volcano plot depicting for each protein the log2 abundance change in the CSF of *iRhom1*$^{-/-}$ compared to littermate control mice and the negative log10 *p*-value (two-sample *t*-test, $N = 4$). Permutation-based false discovery rate (FDR) estimation is visualized with the grey hyperbolic curves. Proteins with a *p*-value below .05 are highlighted with a purple circle and their protein name. Potentially shed proteins are indicated with a filled circle. (E) Potential ADAM17 substrate candidates which show a significant reduction (*p*-value < .05) in *iRhom1*$^{-/-}$ CSF. LAG3 is a known ADAM17 substrate and is highlighted with white letters. (F) The peptide distribution according to the specific protein domains of all ADAM17 substrate candidates was visualized using the web tool Quantitative Analysis of Regulated Intramembrane Proteolysis (QARIP).[85] The number in brackets indicates the number of unique peptides identified for each candidate

and tested whether their iRhom1-dependent shedding indeed depends on ADAM17. Mouse embryonic fibroblasts (MEF) derived from *ADAM17*$^{-/-}$ or *ADAM17*$^{+/+}$ control mice[32] were transiently transfected with constructs encoding a chimeric protein of alkaline phosphate (AP) fused to the ectodomain of the indicated membrane proteins (Figure 4B). Upon shedding, the AP-tagged ectodomain is released into the MEF cell secretome, where it is quantified with an AP activity assay and normalized to the AP activity of the full-length protein in the cell, similar to previous studies using this approach for studying membrane protein shedding.[18,19,22,23,55–59] ADAM17-dependent shedding can be rapidly and reversibly stimulated by a number of physiological stimuli and by the phorbol ester PMA, which is often used as a surrogate for physiological stimulation.[60,61] As positive controls for ADAM17-dependent shedding we used transforming growth factor α (TGF α) and SEMA5B, where PMA increased shedding compared to control, DMSO-treated cells (Figure 4), while this increase was

TABLE 2 List of the six significantly (p-value < .05) reduced potentially shed proteins detected in the CSF of *iRhom1*$^{-/-}$ versus *iRhom1*$^{+/+}$ mice

ProteinAC	Gene name	p-value	Fold change KO versus WT	Topology	AD17 substrate	Neuronal secretome	Brain cell origin[a]
O08644	Ephb6	1.17E−03	0.67	TM1		n.d.	n.d.
Q64449	Mrc2	8.14E−03	0.50	TM1		d.	A, M, N, O
Q61790	Lag3	9.92E−03	0.68	TM1	+	n.d.	M
P35951	Ldlr	1.64E−02	0.64	TM1		sig inc.	N, O
Q6DIB5	Megf10	1.98E−02	0.66	TM1		sig red.	A, M, N, O
O35136	Ncam2	2.33E−02	0.67	GPI		d.	O

Abbreviations: A, astrocyte; d., detected; GPI, GPI-anchored protein; M, microglia; n.d., not detected; N, neuron; O, oligodendrocytes; sign. red., significantly reduced; sign. inc., significantly increased; TM1, transmembrane protein type 1; TM2, transmembrane protein type 2.

[a]According to the brain cell type-resolved secretome resource by Ref. [35]

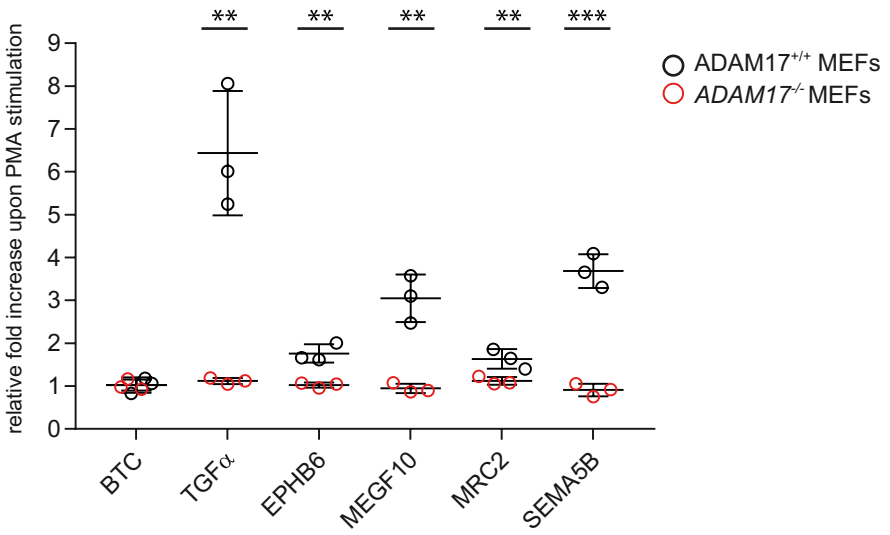

FIGURE 4 iRhom1-dependent brain shedding substrates are substrates for ADAM17. *Adam17*$^{+/+}$ (black) and *Adam17*$^{-/-}$ (red) MEFs overexpressing substrate candidates carrying an alkaline phosphatase (AP)-tag were treated with or without PMA for 45 min ($N = 3$). The AP activity in the conditioned media was normalized to the expression level as well as to the untreated sample. p-values indicated in brackets for all significantly upregulated shed ectodomains upon PMA stimulation: TGFα (1.13E−03), EPHB6 (1.49E−03), MEGF10 (1.42E−04), MRC2 (3.75E−04), SEMA5B (2.9E−04) (unpaired t-test). (**p-value < .01; ***p-value < .001)

abolished in *ADAM17*$^{-/-}$ MEFs, in agreement with previous studies.[22,51,55,61] As a negative control, betacellulin (BTC) was used, which is an established substrate for ADAM10, but not ADAM17.[6,55,62] As expected, PMA did not increase BTC shedding, neither in *ADAM17*$^{+/+}$, nor in *ADAM17*$^{-/-}$ MEFs. Then we tested MEGF10, which had been identified as an iRhom1-dependent shedding substrate both in vitro and in vivo, as well as EphB6 and MRC2, which were shed in an iRhom1-dependent manner in CSF. For all three proteins, PMA significantly increased their shedding and this increase was not seen in *Adam17*$^{-/-}$ MEFs, establishing all three proteins as ADAM17 substrates. Taken together, MEGF10, MRC2, and EPHB6 are validated not only as iRhom1-, but also as ADAM17-dependent shedding substrates.

4 | DISCUSSION

The pseudoproteases iRhom1 and iRhom2 act as non-proteolytic subunits of an iRhom/ADAM17 protease complex.[16,17] While both iRhoms are co-expressed in most cell types, myeloid cells appear to only express iRhom2. Therefore, single deficiency of iRhom2 leads to a complete loss of ADAM17 activity in myeloid cells.[14,15,26] As a result, proinflammatory ADAM17 substrates such as TNFα, HB-EGF and the IL-6R are no longer shed. Consequently, iRhom2-deficient mice are protected from several TNF-dependent inflammatory and metabolic disorders, making iRhom2 a major drug target for these diseases.[14,26,63–68] Another organ with expression of predominantly a single iRhom is the brain, where mostly iRhom1, but only very

little iRhom2 is expressed.[16,17] Our study demonstrates that iRhom1 is widely expressed in the brain and controls the ectodomain shedding of brain membrane proteins, including EphB6, MRC2, and MEGF10.

MEGF10 was identified in our study as a new ADAM17 substrate that requires iRhom1 for its shedding both in vitro and in vivo. In the brain, MEGF10 is expressed in astrocytes, but also other cell types, including neurons.[69,70] MEGF10 acts as a phagocytic receptor contributing to removal of the Alzheimer's disease-linked amyloid β peptide and of apoptotic neurons.[71–75] Additionally, MEGF10 is linked to activity-dependent synapse pruning and myopathies and may act as a ligand in neuronal patterning in the retina.[70,71,76] Shedding of MEGF10 has not yet been studied, but occurs in astrocytes, microglia, neurons, and oligodendrocytes, according to a recently published resource describing the cell type-resolved mouse brain secretome.[35] At present it is not known whether ADAM17/iRhom1-mediated shedding is a mechanism to control MEGF10 function, but this appears possible given the general role of shedding in modulating membrane protein function.[1]

Besides MEGF10, we also identified EphB6 and Mrc2 as novel ADAM17/iRhom1-dependent shedding substrates. EphB6 belongs to the family of erythropoietin-producing hepatoma (Eph) receptors and is linked to various types of cancers.[77] In contrast with other Eph receptors, EphB6 lacks a functional kinase domain and little is known about its molecular function. Shedding of EphB6 was not previously described. MRC2 is also referred to as C-type mannose receptor 2, uPARAP or Endo180 and acts as a receptor endocytosing collagen.[78] MRC2 was previously described to undergo shedding from tumor cell lines[79] and was detected to be shed from different brain cell types,[35] but the underlying mechanisms or the contributing protease were not known.

ADAM17 can constitutively cleave substrates, but it also functions as a post-translationally regulated sheddase for numerous membrane proteins after rapid and reversible stimulation by a number of physiological stimuli or by the phorbol ester PMA.[22,55,61] Thus, it is well-conceivable that more iRhom1/ADAM17-dependent shedding substrates exist in brain and that their discovery requires appropriate ADAM17/ iRhom1 stimulation in vitro or in vivo.

In our study, we analyzed the CSF from one of the distinct existing iRhom1-deficient mouse lines.[16,17,80] The mouse line used in our study lacks exons 4 to 11 and shows no evident spontaneous pathological phenotype and is viable and fertile, despite the lack of mature ADAM17 in the brain.[16] A similar phenotype was reported for another iRhom1-deficient line in which exons 2 and 3 were deleted,[80] whereas two other lines showed brain hemorrhages, hypertrophy, and fibrosis in the heart and postnatal lethality[16,17,80] so that they do not reach the adult age required for CSF sampling. The molecular cause of the two distinct phenotypes is not yet clear, but appears to correlate with how many exons of the iRhom1 gene were deleted.[80]

ADAM17 can contribute to CNS myelination and remyelination, apparently in both neurons and oligodendrocytes.[44–46] Given this link of ADAM17 to myelination, it is interesting to note that we did not observe obvious differences in spinal cord myelination in adult mice, although we found the mature, proteolytically active form of ADAM17 to be nearly completely lacking in *iRhom1*$^{-/-}$ mouse brain, in agreement with a previous study.[16] Potentially, the increased abundance of ADAM10 and BACE1, which we observed in *iRhom1*$^{-/-}$ neurons, compensates for the loss of ADAM17, because both ADAM10 and BACE1 as well as their substrates can positively influence myelination, for example, through cleavage of neuregulin-1 or DR6.[2,81–83]

The increased ADAM10 and BACE1 levels in primary *iRhom1*$^{-/-}$ neurons correlated with enhanced shedding of several ADAM10 and BACE1 substrates in the primary neuron secretome, but an increased shedding of these substrates was not seen in the CSF of *iRhom1*$^{-/-}$ mice. Similarly, CADM4, OMG, and PLD3 showed reduced shedding in the neuronal *iRhom1*$^{-/-}$ secretome, but no change in the CSF of *iRhom1*$^{-/-}$ mice. This apparent difference may be due to the fact, that CSF does not only contain proteins secreted from neurons, but also from other brain cell types, including astrocytes, microglia, oligodendrocytes, and choroid plexus epithelial cells as well as proteins crossing the blood brain barrier. CADM4, OMG, and PLD3 are not only shed from neurons, but also other brain cell types.[35] As the major protease shedding a membrane protein may differ among cell types,[1] it appears possible that shedding of these three proteins in vivo is iRhom1-dependent in neurons, but not in other brain cell types, where potentially proteases other than ADAM17 may cleave these membrane proteins. Because the non-neuronal cells outnumber the neurons, there may be no net change in shedding of these proteins, when analyzing whole CSF. Likewise, the upregulation of ADAM10 and BACE1 may only be relevant in neurons, but not in other brain cell types. Alternatively, the upregulation of ADAM10 and BACE1 may be seen in primary neurons in vitro, but not in vivo. A similar finding has been reported for primary microglia, which can change their expression profile when taken into culture in vitro and then become more macrophage-like.[84]

In summary, our study provides the first characterization of iRhom1 expression and function in the murine brain. We demonstrate that iRhom1 is widely expressed in brain and across all ages studied. This study also reveals a role for iRhom1 in controlling ADAM17-mediated

ectodomain shedding of membrane proteins in the CNS, such as EPHB6, MEGF10, and MRC2. Because these membrane proteins, in particular MEGF10, have essential functions in the nervous system, it is possible that—through control of their shedding—iRhom1 has fundamental functions in brain homeostasis.

ACKNOWLEDGEMENTS

We thank Katrin Moschke for excellent help with the developmental iRhom1 expression analysis. This work was funded by the Deutsche Forschungsgemeinschaft (DFG, German Research Foundation) under Germany's Excellence Strategy within the framework of the Munich Cluster for Systems Neurology (EXC 2145 SyNergy–ID 390857198) and within project 263531414/FOR 2290 and by the BMBF through project CLINSPECT-M (FKZ161L0214C, ClinspectM), and NIH R35 GM134907 to CPB. JT was awarded the Boehringer Ingelheim Fonds (BIF) PhD fellowship.

DISCLOSURES

Dr Blobel holds a patent on a method of identifying agents for combination with inhibitors of iRhoms. Dr Blobel and the Hospital for Special Surgery have identified iRhom2 inhibitors together with the start-up company SciRhom which they co-founded in Munich to commercialize these inhibitors. The other authors declare to have no conflict of interest.

AUTHOR CONTRIBUTIONS

Johanna Tüshaus, Carl P. Blobel, and Stefan F. Lichtenthaler conceived the study, designed the experiments, and analyzed the data. Johanna Tüshaus performed most of the experiments. Johanna Tüshaus and Stephan A. Müller performed the mass spectrometry analyses. Joshua Shrouder and Nikolaus Plesnila performed brain vessel analysis. Martina Arends and Mikael Simons did the myelination analysis. Johanna Tüshaus, Carl P. Blobel, and Stefan F. Lichtenthaler wrote the manuscript; all authors contributed to editing and manuscript revisions.

REFERENCES

1. Lichtenthaler SF, Lemberg MK, Fluhrer R. Proteolytic ectodomain shedding of membrane proteins in mammals-hardware, concepts, and recent developments. *EMBO J*. 2018;37:e99456.
2. Hsia HE, Tushaus J, Brummer T, Zheng Y, Scilabra SD, Lichtenthaler SF. Functions of 'A disintegrin and metalloproteases (ADAMs)' in the mammalian nervous system. *Cell Mol Life Sci*. 2019;76:3055-3081.
3. Murphy G. The ADAMs: signalling scissors in the tumour microenvironment. *Nat Rev Cancer*. 2008;8:932-941.
4. Jones JC, Rustagi S, Dempsey PJ. ADAM proteases and gastrointestinal function. *Annu Rev Physiol*. 2016;78:243-276.
5. Dreymueller D, Uhlig S, Ludwig A. ADAM-family metalloproteinases in lung inflammation: potential therapeutic targets. *Am J Physiol Lung Cell Mol Physiol*. 2015;308:L325-L343.
6. Blobel CP. ADAMs: key components in EGFR signalling and development. *Nat Rev Mol Cell Biol*. 2005;6:32-43.
7. Zunke F, Rose-John S. The shedding protease ADAM17: physiology and pathophysiology. *Biochim Biophys Acta Mol Cell Res*. 2017;1864:2059-2070.
8. Jackson LF, Qiu TH, Sunnarborg SW, et al. Defective valvulogenesis in HB-EGF and TACE-null mice is associated with aberrant BMP signaling. *EMBO J*. 2003;22:2704-2716.
9. Peschon JJ, Slack JL, Reddy P, et al. An essential role for ectodomain shedding in mammalian development. *Science*. 1998;282:1281-1284.
10. Mine N, Iwamoto R, Mekada E. HB-EGF promotes epithelial cell migration in eyelid development. *Development*. 2005;132:4317-4326.
11. Sternlicht MD, Sunnarborg SW, Kouros-Mehr H, Yu Y, Lee DC, Werb Z. Mammary ductal morphogenesis requires paracrine activation of stromal EGFR via ADAM17-dependent shedding of epithelial amphiregulin. *Development*. 2005;132:3923-3933.
12. Black RA, Rauch CT, Kozlosky CJ, et al. A metalloproteinase disintegrin that releases tumour-necrosis factor-alpha from cells. *Nature*. 1997;385:729-733.
13. Moss ML, Jin SL, Milla ME, et al. Cloning of a disintegrin metalloproteinase that processes precursor tumour-necrosis factor-alpha. *Nature*. 1997;385:733-736.
14. McIlwain DR, Lang PA, Maretzky T, et al. iRhom2 regulation of TACE controls TNF-mediated protection against Listeria and responses to LPS. *Science*. 2012;335:229-232.
15. Adrain C, Zettl M, Christova Y, Taylor N, Freeman M. Tumor necrosis factor signaling requires iRhom2 to promote trafficking and activation of TACE. *Science*. 2012;335:225-228.
16. Li X, Maretzky T, Weskamp G, et al. iRhoms 1 and 2 are essential upstream regulators of ADAM17-dependent EGFR signaling. *Proc Natl Acad Sci USA*. 2015;112:6080-6085.
17. Christova Y, Adrain C, Bambrough P, Ibrahim A, Freeman M. Mammalian iRhoms have distinct physiological functions including an essential role in TACE regulation. *EMBO Rep*. 2013;14:884-890.
18. Oikonomidi I, Burbridge E, Cavadas M, et al. iTAP, a novel iRhom interactor, controls TNF secretion by policing the stability of iRhom/TACE. *eLife*. 2018;7:e35032.
19. Kunzel U, Grieve AG, Meng Y, Sieber B, Cowley SA, Freeman M. FRMD8 promotes inflammatory and growth factor signalling by stabilising the iRhom/ADAM17 sheddase complex. *eLife*. 2018;7:e35012.
20. Vinothkumar KR, Strisovsky K, Andreeva A, Christova Y, Verhelst S, Freeman M. The structural basis for catalysis and substrate specificity of a rhomboid protease. *EMBO J*. 2010;29:3797-3809.
21. Li X, Maretzky T, Perez-Aguilar JM, et al. Structural modeling defines transmembrane residues in ADAM17 that are crucial for Rhbdf2-ADAM17-dependent proteolysis. *J Cell Sci*. 2017;130:868-878.
22. Tang B, Li X, Maretzky T, et al. Substrate-selective protein ectodomain shedding by ADAM17 and iRhom2 depends on their juxtamembrane and transmembrane domains. *FASEB J*. 2020;34:4956-4969.

23. Maretzky T, McIlwain DR, Issuree PD, et al. iRhom2 controls the substrate selectivity of stimulated ADAM17-dependent ectodomain shedding. *Proc Natl Acad Sci USA*. 2013;110:11433-11438.
24. Dulloo I, Muliyil S, Freeman M. The molecular, cellular and pathophysiological roles of iRhom pseudoproteases. *Open Biol*. 2019;9:190003.
25. Lichtenthaler SF, O'Hara BF, Blobel CP. iRhoms in the brain—a new frontier? *Cell Cycle*. 2015;14:3003-3004.
26. Issuree PD, Maretzky T, McIlwain DR, et al. iRHOM2 is a critical pathogenic mediator of inflammatory arthritis. *J Clin Invest*. 2013;123:928-932.
27. Zellner A, Scharrer E, Arzberger T, et al. CADASIL brain vessels show a HTRA1 loss-of-function profile. *Acta Neuropathol*. 2018;136:111-125.
28. Rudan Njavro J, Klotz J, Dislich B, et al. Mouse brain proteomics establishes MDGA1 and CACHD1 as in vivo substrates of the Alzheimer protease BACE1. *FASEB J*. 2020;34:2465-2482.
29. Pigoni M, Wanngren J, Kuhn PH, et al. Seizure protein 6 and its homolog seizure 6-like protein are physiological substrates of BACE1 in neurons. *Mol Neurodegener*. 2016;11:67.
30. Weskamp G, Tushaus J, Li D, et al. ADAM17 stabilizes its interacting partner inactive Rhomboid 2 (iRhom2) but not inactive Rhomboid 1 (iRhom1). *J Biol Chem*. 2020;295:4350-4358.
31. Schlöndorff J, Becherer JD, Blobel CP. Intracellular maturation and localization of the tumour necrosis factor alpha convertase (TACE). *Biochem J*. 2000;347(pt 1):131-138.
32. Horiuchi K, Le Gall S, Schulte M, et al. Substrate selectivity of epidermal growth factor-receptor ligand sheddases and their regulation by phorbol esters and calcium influx. *Mol Biol Cell*. 2007;18:176-188.
33. Kuhn PH, Koroniak K, Hogl S, et al. Secretome protein enrichment identifies physiological BACE1 protease substrates in neurons. *EMBO J*. 2012;31:3157-3168.
34. Brummer T, Müller SA, Pan-Montojo F, et al. NrCAM is a marker for substrate-selective activation of ADAM10 in Alzheimer's disease. *EMBO Mol Med*. 2019;11:e9695.
35. Tüshaus J, Müller SA, Kataka ES, et al. An optimized quantitative proteomics method establishes the cell type-resolved mouse brain secretome. *EMBO J*. 2020;39:e105693.
36. Rappsilber J, Ishihama Y, Mann M. Stop and go extraction tips for matrix-assisted laser desorption/ionization, nanoelectrospray, and LC/MS sample pretreatment in proteomics. *Anal Chem*. 2003;75:663-670.
37. Liu L, Duff K. A technique for serial collection of cerebrospinal fluid from the cisterna magna in mouse. *J Vis Exp*. 2008;21:960.
38. Lim NK, Moestrup V, Zhang X, Wang WA, Møller A, Huang FD. An improved method for collection of cerebrospinal fluid from anesthetized mice. *J Vis Exp*. 2018. https://doi.org/10.3791/56774.
39. Tüshaus J, Kataka ES, Zaucha J, Frishman D, Müller SA, Lichtenthaler SF. Neuronal differentiation of LUHMES cells induces substantial changes of the proteome. *Proteomics*. 2021;21:e2000174.
40. Cox J, Neuhauser N, Michalski A, Scheltema RA, Olsen JV, Mann M. Andromeda: a peptide search engine integrated into the MaxQuant environment. *J Proteome Res*. 2011;10:1794-1805.
41. Bruderer R, Bernhardt OM, Gandhi T, Reiter L. High-precision iRT prediction in the targeted analysis of data-independent acquisition and its impact on identification and quantitation. *Proteomics*. 2016;16:2246-2256.
42. Sharma K, Schmitt S, Bergner CG, et al. Cell type- and brain region-resolved mouse brain proteome. *Nat Neurosci*. 2015;18:1819-1831.
43. Zhang Y, Chen K, Sloan SA, et al. An RNA-sequencing transcriptome and splicing database of glia, neurons, and vascular cells of the cerebral cortex. *J Neurosci*. 2014;34:11929-11947.
44. Palazuelos J, Crawford HC, Klingener M, et al. TACE/ADAM17 is essential for oligodendrocyte development and CNS myelination. *J Neurosci*. 2014;34:11884-11896.
45. Palazuelos J, Klingener M, Raines EW, Crawford HC, Aguirre A. Oligodendrocyte regeneration and CNS remyelination require TACE/ADAM17. *J Neurosci*. 2015;35:12241-12247.
46. Fredrickx E, Colombo E, Canevazzi P, et al. Ablation of neuronal ADAM17 impairs oligodendrocyte differentiation and myelination. *Glia*. 2020;68:1148-1164.
47. Weskamp G, Mendelson K, Swendeman S, et al. Pathological neovascularization is reduced by inactivation of ADAM17 in endothelial cells but not in pericytes. *Circ Res*. 2010;106:932-940.
48. Canault M, Certel K, Schatzberg D, Wagner DD, Hynes RO. The lack of ADAM17 activity during embryonic development causes hemorrhage and impairs vessel formation. *PLoS ONE*. 2010;5:e13433.
49. Kuhn PH, Voss M, Haug-Kroper M, et al. Secretome analysis identifies novel signal peptide peptidase-like 3 (Sppl3) substrates and reveals a role of Sppl3 in multiple Golgi glycosylation pathways. *Mol Cell Proteomics*. 2015;14:1584-1598.
50. Kuhn PH, Colombo AV, Schusser B, et al. Systematic substrate identification indicates a central role for the metalloprotease ADAM10 in axon targeting and synapse function. *eLife*. 2016;5:e12748.
51. Browne K, Wang W, Liu RQ, Piva M, O'Connor TP. Transmembrane semaphorin5B is proteolytically processed into a repulsive neural guidance cue. *J Neurochem*. 2012;123:135-146.
52. Pigoni M, Hsia HE, Hartmann J, et al. Seizure protein 6 controls glycosylation and trafficking of kainate receptor subunits GluK2 and GluK3. *EMBO J*. 2020;39:e103457.
53. Brummer T, Pigoni M, Rossello A, et al. The metalloprotease ADAM10 (a disintegrin and metalloprotease 10) undergoes rapid, postlysis autocatalytic degradation. *FASEB J*. 2018;32:3560-3573.
54. Li N, Wang Y, Forbes K, et al. Metalloproteases regulate T-cell proliferation and effector function via LAG-3. *EMBO J*. 2007;26:494-504.
55. Sahin U, Weskamp G, Kelly K, et al. Distinct roles for ADAM10 and ADAM17 in ectodomain shedding of six EGFR ligands. *J Cell Biol*. 2004;164:769-779.
56. Grieve AG, Xu H, Kunzel U, Bambrough P, Sieber B, Freeman M. Phosphorylation of iRhom2 at the plasma membrane controls mammalian TACE-dependent inflammatory and growth factor signalling. *eLife*. 2017;6:e23968.
57. Sahin U, Blobel CP. Ectodomain shedding of the EGF-receptor ligand epigen is mediated by ADAM17. *FEBS Lett*. 2007;581:41-44.
58. Kuhn PH, Marjaux E, Imhof A, De Strooper B, Haass C, Lichtenthaler SF. Regulated intramembrane proteolysis of the interleukin-1 receptor II by alpha-, beta-, and gamma-secretase. *J Biol Chem*. 2007;282:11982-11995.
59. Lichtenthaler SF, Dominguez DI, Westmeyer GG, et al. The cell adhesion protein P-selectin glycoprotein ligand-1 is

a substrate for the aspartyl protease BACE1. *J Biol Chem*. 2003;278:48713-48719.
60. Lorenzen I, Lokau J, Korpys Y, et al. Control of ADAM17 activity by regulation of its cellular localisation. *Sci Rep*. 2016;6:35067.
61. Le Gall SM, Maretzky T, Issuree PD, et al. ADAM17 is regulated by a rapid and reversible mechanism that controls access to its catalytic site. *J Cell Sci*. 2010;123:3913-3922.
62. Sanderson MP, Erickson SN, Gough PJ, et al. ADAM10 mediates ectodomain shedding of the betacellulin precursor activated by p-aminophenylmercuric acetate and extracellular calcium influx. *J Biol Chem*. 2005;280:1826-1837.
63. Haxaire C, Hakobyan N, Pannellini T, et al. Blood-induced bone loss in murine hemophilic arthropathy is prevented by blocking the iRhom2/ADAM17/TNF-alpha pathway. *Blood*. 2018;132:1064-1074.
64. Qing X, Chinenov Y, Redecha P, et al. iRhom2 promotes lupus nephritis through TNF-alpha and EGFR signaling. *J Clin Invest*. 2018;128:1397-1412.
65. Deng M, Loughran PA, Zhang L, Scott MJ, Billiar TR. Shedding of the tumor necrosis factor (TNF) receptor from the surface of hepatocytes during sepsis limits inflammation through cGMP signaling. *Sci Signal*. 2015;8:ra11.
66. Badenes M, Amin A, Gonzalez-Garcia I, et al. Deletion of iRhom2 protects against diet-induced obesity by increasing thermogenesis. *Mol Metab*. 2020;31:67-84.
67. Skurski J, Penniman CM, Geesala R, et al. Loss of iRhom2 accelerates fat gain and insulin resistance in diet-induced obesity despite reduced adipose tissue inflammation. *Metabolism*. 2020;106:154194.
68. Geesala R, Schanz W, Biggs M, et al. Loss of RHBDF2 results in an early-onset spontaneous murine colitis. *J Leukoc Biol*. 2019;105:767-781.
69. Fujita Y, Maeda T, Kamaishi K, et al. Expression of MEGF10 in cholinergic and glutamatergic neurons. *Neurosci Lett*. 2017;653:25-30.
70. Kay JN, Chu MW, Sanes JR. MEGF10 and MEGF11 mediate homotypic interactions required for mosaic spacing of retinal neurons. *Nature*. 2012;483:465-469.
71. Lee JH, Kim JY, Noh S, et al. Astrocytes phagocytose adult hippocampal synapses for circuit homeostasis. *Nature*. 2021;590:612-617.
72. Fujita Y, Maeda T, Sato C, et al. Engulfment of toxic amyloid β-protein in neurons and astrocytes mediated by MEGF10. *Neuroscience*. 2020;443:1-7.
73. Iram T, Ramirez-Ortiz Z, Byrne MH, et al. Megf10 is a receptor for C1Q that mediates clearance of apoptotic cells by astrocytes. *J Neurosci*. 2016;36:5185-5192.
74. Singh TD, Park SY, Bae JS, et al. MEGF10 functions as a receptor for the uptake of amyloid-β. *FEBS Lett*. 2010;584:3936-3942.
75. Chung WS, Clarke LE, Wang GX, et al. Astrocytes mediate synapse elimination through MEGF10 and MERTK pathways. *Nature*. 2013;504:394-400.
76. Logan CV, Lucke B, Pottinger C, et al. Mutations in MEGF10, a regulator of satellite cell myogenesis, cause early onset myopathy, areflexia, respiratory distress and dysphagia (EMARDD). *Nat Genet*. 2011;43:1189-1192.
77. Liang LY, Patel O, Janes PW, Murphy JM, Lucet IS. Eph receptor signalling: from catalytic to non-catalytic functions. *Oncogene*. 2019;38:6567-6584.
78. Melander MC, Jürgensen HJ, Madsen DH, Engelholm LH, Behrendt N. The collagen receptor uPARAP/Endo180 in tissue degradation and cancer (Review). *Int J Oncol*. 2015;47:1177-1188.
79. Palmieri C, Caley MP, Purshouse K, et al. Endo180 modulation by bisphosphonates and diagnostic accuracy in metastatic breast cancer. *Br J Cancer*. 2013;108:163-169.
80. Hosur V, Low BE & Li D, et al. Genes adapt to outsmart gene targeting strategies in mutant mouse strains by skipping exons to reinitiate transcription and translation. *Genome Biol*. 2020;21:168.
81. Colombo A, Hsia H-E, Wang M, et al. Non-cell-autonomous function of DR6 in Schwann cell proliferation. *EMBO J*. 2018;37:e97390.
82. Willem M, Garratt AN, Novak B, et al. Control of peripheral nerve myelination by the beta-secretase BACE1. *Science*. 2006;314:664-666.
83. Hu X, Hicks CW, He W, et al. Bace1 modulates myelination in the central and peripheral nervous system. *Nat Neurosci*. 2006;9:1520-1525.
84. Gosselin D, Skola D, Coufal NG, et al. An environment-dependent transcriptional network specifies human microglia identity. *Science*. 2017;356:eaal3222.
85. Ivankov DN, Bogatyreva NS, Hönigschmid P, et al. QARIP: a web server for quantitative proteomic analysis of regulated intramembrane proteolysis. *Nucleic Acids Res*. 2013;41:W459-W464.

SUPPORTING INFORMATION

Additional Supporting Information may be found in the online version of the article at the publisher's website.

How to cite this article: Tüshaus J, Müller SA, Shrouder J, et al. The pseudoprotease iRhom1 controls ectodomain shedding of membrane proteins in the nervous system. *FASEB J*. 2021;35:e21962. doi:10.1096/fj.202100936R